GEOPHYSICS, VOL. 85, NO. 2 (MARCH-APRIL 2020); P. S65–S70, 6 FIGS.
10.1190/GEO2019-0327.1

A field data example of Marchenko multiple elimination

Lele Zhang[1] and Evert Slob[1]

ABSTRACT

Internal multiple reflections have been widely considered as coherent noise in measured seismic data, and many approaches have been developed for their attenuation. The Marchenko multiple elimination (MME) scheme eliminates internal multiple reflections without model information or adaptive subtraction. This scheme was originally derived from coupled Marchenko equations, but it was modified to make it model independent. It filters primary reflections with their two-way traveltimes and physical amplitudes from measured seismic data. The MME scheme is applied to a deepwater field data set from the Norwegian North Sea to evaluate its success in removing internal multiple reflections. The result indicates that most internal multiple reflections are successfully removed and primary reflections masked by overlapping internal multiple reflections are recovered.

INTRODUCTION

Standard migration schemes map all of the reflections in the data into reflectors in the model domain if they are all primary reflections. These schemes assume that all events in the measured data are reflected only once in the subsurface. Because of this assumption, the measured seismic data should be preprocessed before being migrated by standard migration schemes. Therefore, multiple reflection elimination schemes play a crucial role for standard migration schemes. To date, several approaches have been developed to deal with multiple reflections. Some focus on free-surface-multiple reflections, whereas others focus on internal multiple reflections.

Free-surface-multiple reflections can be strong enough to cause artifacts in the image from marine and land data such that much attention has been attracted from industry and academia. Free-surface-multiple elimination (SRME) (Verschuur et al., 1992) and estimation of primaries by sparse inversion (EPSI) (van Groenestijn and Verschuur, 2009) are the two schemes that have been widely accepted as robust tools for free-surface-multiple attenuation in industry. For SRME, all orders of free-surface-multiple reflections are predicted and a minimum-energy criterion is used to subtract predicted events from the measured data. The EPSI scheme replaces the two-stage processing of SRME, prediction, and adaptive subtraction by an inversion scheme based on the full-waveform inversion approach (van Groenestijn and Verschuur, 2009). Both have achieved success on field data sets. Another strategy is to image the primary and free-surface multiple reflections simultaneously (Brown and Guitton, 2005; Whitmore et al., 2010; Verschuur and Berkhout, 2011; Wang et al., 2014, 2017; Lu et al., 2015), where free-surface multiple reflections give extended illumination of the subsurface. However, crosstalk is present in the resulting image as coherent noise.

Less effort has been devoted to deal with internal multiple reflections. As pioneers, Araújo et al. (1994) derive an internal multiple attenuation scheme from the inverse scattering series (ISS). This is the first data-driven scheme that was developed by Weglein et al. (1997) and modified by Ten Kroode (2002) and Löer et al. (2016). Internal multiple elimination (IME) is a layer-related scheme extended from SRME (Berkhout and Verschuur, 1997). The IME scheme downward extrapolates shot records to a virtual surface and attenuates internal multiple reflections related to that surface. Therefore, velocity information is required for its implementation. The ISS and IME schemes have been demonstrated on numerical and field data sets (Matson et al., 1999; Verschuur and Berkhout, 2005; Luo et al., 2011). Adaptive subtraction is needed for both schemes to achieve a multiple-attenuated data set because of the approximate nature of the predicted events. Using internal multiple reflections in imaging is done via full wavefield migration, a data-consistent closed-loop scheme (Berkhout, 2014). Davydenko and Verschuur (2018) present a field data application.

Recently, Marchenko redatuming schemes have been proposed to remove internal multiple reflections and create images free from artifacts (Slob et al., 2014; Wapenaar et al., 2014). Meles et al. (2015) combine convolutional interferometry with the Marchenko scheme to give an internal multiple reflection attenuation scheme.

Manuscript received by the Editor 26 May 2019; revised manuscript received 5 September 2019; published ahead of production 30 October 2019; published online 9 January 2020.
[1]Delft University of Technology, 2628 CN Delft, The Netherlands. E-mail: l.zhang-1@tudelft.nl (corresponding author); e.c.slob@tudelft.nl.

Staring et al. (2018) propose to attenuate the first-order internal multiple reflections using an adaptive Marchenko double-focusing method. Model information and adaptive subtraction are required for the implementation of these schemes. Zhang and Staring (2018) modify a Marchenko multiple elimination (MME) scheme (van der Neut and Wapenaar, 2016), which in theory removes all orders of internal multiple reflections without model information or adaptive subtraction. The MME scheme has been extended to also account for transmission loss in primary reflections and free-surface multiple reflections (Zhang and Slob, 2019). Thus, free-surface and internal multiple reflections can be removed and transmission loss in primary reflections can be compensated for in one step without model information or adaptive subtraction.

In this paper, the MME scheme is applied to a deepwater field data set from the Norwegian North Sea. It is the first field data example to validate its capabilities for removal of internal multiple reflections without model information or adaptive subtraction. The paper is organized as follows. In the "Theory" section, we give a brief overview of the theory of the MME scheme. The detailed theory can be found in Zhang and Staring (2018). In the "Field example" section, we apply the MME scheme to a field data set for internal multiple reflection elimination. The performance of the MME scheme is analyzed in the "Discussion" section, and we end with our conclusions.

THEORY

We follow Zhang et al. (2019b) to give the equations of the MME scheme in the iterative form because they can be implemented,

$$R_t(\mathbf{x}_0', \mathbf{x}_0'', t) = R(\mathbf{x}_0', \mathbf{x}_0'', t) + \sum_{m=1}^{\infty} M_m(\mathbf{x}_0', \mathbf{x}_0'', t), \quad (1)$$

with

$$\begin{aligned} M_m(\mathbf{x}_0', \mathbf{x}_0'', t) = & \int_0^{+\infty} \mathrm{d}t' \int_{\partial \mathbf{D}_0} \mathrm{d}\mathbf{x}_0''' R(\mathbf{x}_0', \mathbf{x}_0''', t') H(t - t' - \tau) \\ & \times \int_0^{+\infty} \mathrm{d}t'' \int_{\partial \mathbf{D}_0} \mathrm{d}\mathbf{x}_0 R(\mathbf{x}_0''', \mathbf{x}_0, t'') H(t' - t'' - \tau) \\ & \times M_{m-1}(\mathbf{x}_0, \mathbf{x}_0'', t - t' + t'') \end{aligned} \quad (2)$$

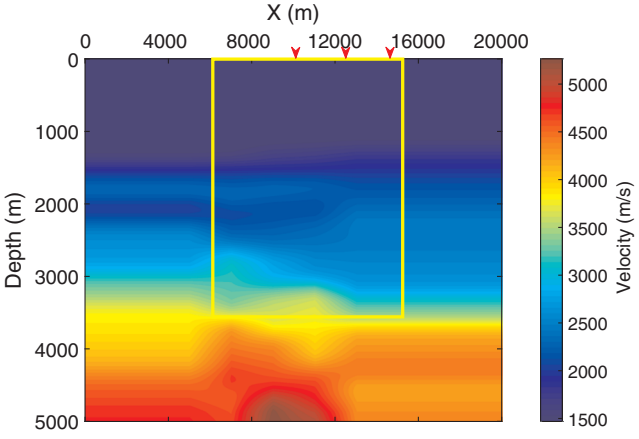

Figure 1. The macrovelocity model used to migrate the data sets before and after internal multiple reflection elimination. The red arrows indicate the source positions of the shot gathers shown in Figure 2, and the yellow box marks the imaged target zone.

and

$$M_0 = R, \quad (3)$$

where $R(\mathbf{x}_0', \mathbf{x}_0, t)$ denotes the impulse reflection response with the source at $\mathbf{x}_0$ and the receiver at $\mathbf{x}_0'$; both are at the acquisition surface. The summation of M_m with $m = 1, \ldots, \infty$ predicts all orders of internal multiple reflections with correct amplitudes, and the retrieved multiple-free data set is denoted by R_t. The function H indicates the Heaviside function to impose the truncation time window $(\tau, t - \tau)$, and the window $(\tau, t - \tau)$ is offset independent; τ indicates a small positive value. Equation 3 shows that the impulse reflection response is the start of the MME scheme given in equation 1.

We assume that the input impulse reflection response R contains only primary and internal multiple reflections. Thus, the measured reflection response is required to be deconvolved for the source time signature and attenuated for free-surface-related multiple reflections for the implementation of the MME scheme. Refracted and scattered waves in the measured data are not accounted for by the MME scheme, and their effects have been analyzed in Zhang et al. (2019a). The truncation time t is the time instant at which the equation is evaluated with a constant shift τ, which can be taken as the half-wavelength of the source signature. No adaptive filtering or subsurface information is required for the implementation of the MME scheme.

FIELD EXAMPLE

In this section, we describe application of the MME scheme to a 2D streamer field data set provided by Equinor, which was acquired in the Norwegian Sea in 1994. There are 399 shot gathers and 399 traces per gather in the field data set. The spatial sampling of the sources and receivers is 25 m. For this field data set, as illustrated in Davydenko and Verschuur (2018), the following preprocessing has been done:

1) Mute the direct wave.
2) Interpolate the missing near-offset traces using the parabolic Radon transform (Kabir and Verschuur, 1995).
3) Multiply the data with $\sqrt{t}$ to mimic 2D geometric spreading.
4) Apply the source signature deconvolution for removing the air-gun bubble effect.
5) Attenuate the free-surface-related multiple reflections using SRME.

   Note that the water bottom (1.5 km) is deep enough such that free-surface-related multiple reflections arrive after 4 s, which is after the maximum time that we use to show our results. In this time interval, only primary and internal multiple reflections occur. Thus, it guarantees that there can be no residuals of surface-related-multiple reflections in this part of the data after SRME. Receiver deghosting was not performed on the measured data set because the vertical arrival assumption for the ghost would not cause larger errors in the deep water. Due to attenuation, the source ghost, imperfect source signature deconvolution, and 3D effect compensation, the amplitude information does not meet the requirement of the MME scheme and we applied a global scaling factor for the correction. The global scaling factor was estimated from the difference of amplitude between the predicted and actual events.

Figure 1 shows a macrovelocity model of the target basin where the data set was acquired. This model is not used for internal multiple elimination and merely serves to illustrate the environment. The yellow box marks the imaged target zone. The red arrows indicate the source positions of the three shot gathers that are shown in Figure 2a, 2d, and 2g. Note that, between 2.5 and 3.5 s, internal multiple reflections indicated by the red arrows are present. We use the MME scheme given in equation 1 to remove internal multiple reflections in the field data set. The predicted internal multiple reflections are given in Figure 2b, 2e, and 2h, whereas the corresponding multiple attenuated gathers are presented in Figure 2c, 2f, and 2i. These results show that internal multiple reflections, indicated by the red arrows in Figure 2a, 2d, and 2g, are successfully predicted by the MME scheme as shown in Figure 2b, 2e, and 2h. Correspondingly, these events are removed or attenuated in the resulting gathers shown in Figure 2c, 2f, and 2i. Note that the events indicated by the green arrows in Figure 2c and 2f are not visibly present in Figure 2a and 2d but present in Figure 2b and 2e. It does not necessarily imply that the MME scheme introduces new events. It is caused by the fact that these two events are canceled by internal multiple reflections in the original shot gathers and after internal multiple reflection elimination; these canceled primary reflections are recovered in the resulting shot gathers. No model information or adaptive subtraction is used in the implementation of the MME scheme, such that masked primary reflections are recovered.

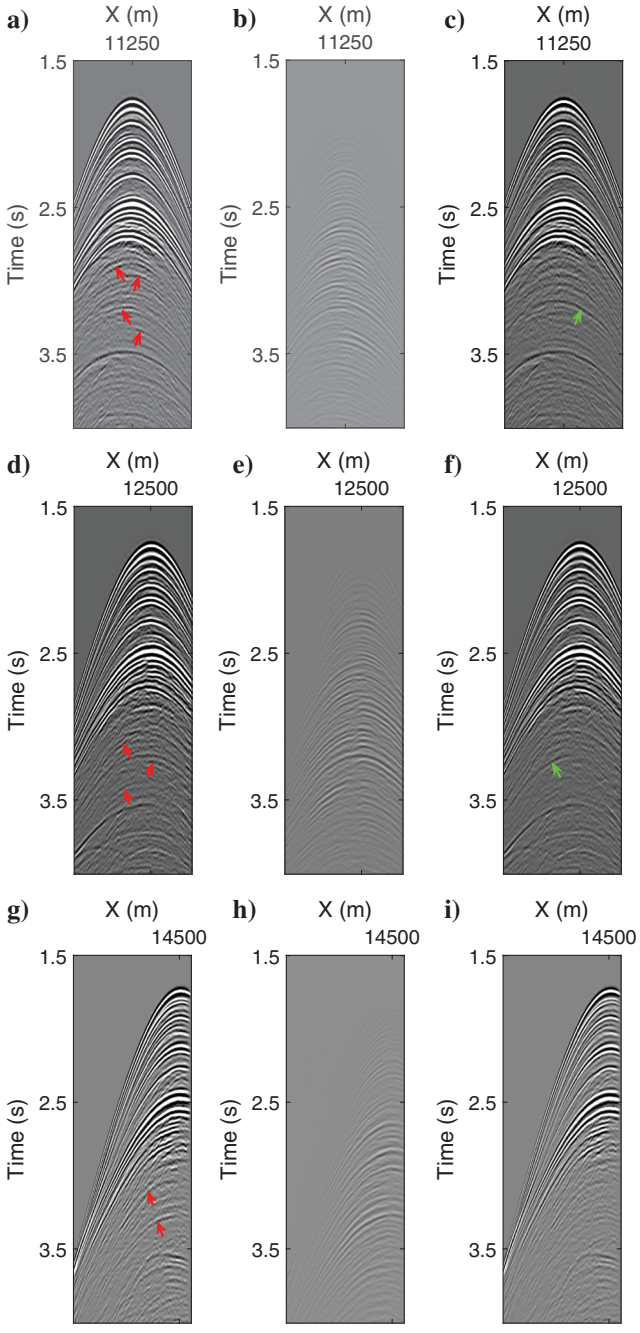

Figure 2. The subparts (a, d, and g) represent the original shot records, (b, e, and h) represent the predicted internal multiple reflections by the MME scheme, and (c, f, and i) represent the corresponding multiple-eliminated shot records. The red arrows indicate internal multiple reflections, and the green arrows indicate primary reflections recovered after the processing.

We use the macrovelocity model given in Figure 1 in a one-way wave-equation migration scheme to migrate the data sets before and after internal multiple reflection elimination. The resulting images are given in Figure 3a and 3b. The red boxes numbered 1, 2, and 3 mark the zones where internal multiple reflection-related artifacts are visibly present in Figure 3a and are almost absent in Figure 3b. We give the magnified portions separately in Figures 4, 5, and 6 of

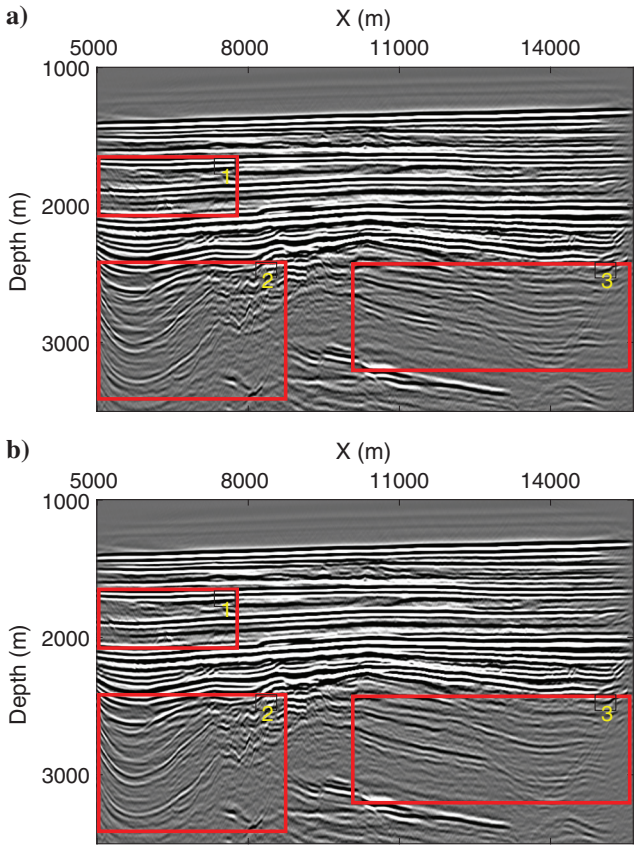

Figure 3. Images from (a) the original measured field data set and (b) the resulting data set of the MME scheme. The numbered red boxes mark zones that are magnified in Figures 4–6 for detailed comparison.

boxes 1–3, respectively, for detailed comparison. In Figure 4, the internal multiple reflection-related artifact, indicated by the red arrow in Figure 4a and 4c, is effectively attenuated with a weak residual as shown in Figure 4b. In Figure 5, the artifacts arising from overburden multiple scattering, indicated by the red arrows in Figure 5a, are successfully removed as shown in Figure 5b. In the part highlighted by the red circle in Figure 5b, the artifacts overlapped with the images from primary reflections are successfully removed as well and the images from primary reflections are well-recovered.

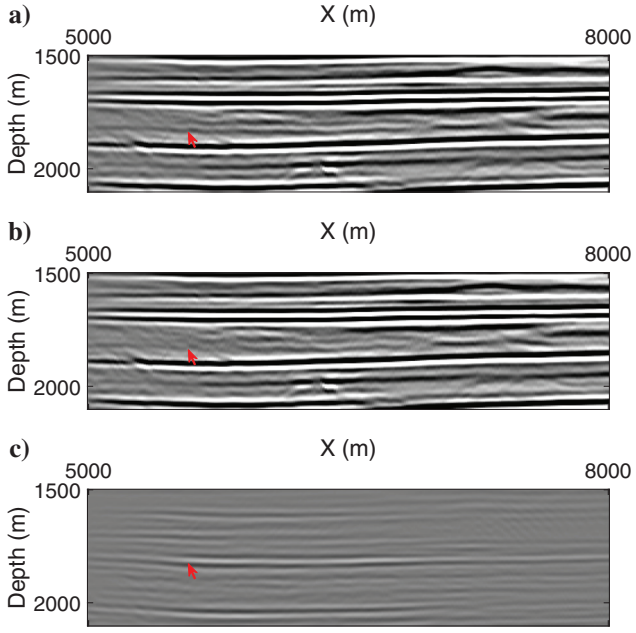

Figure 4. (a) The magnified portion of the zone 1 in Figure 3a, (b) the magnified portion of the zone 1 in Figure 3b, and (c) difference between (a and b). The red arrows indicate the artifact due to internal multiple reflection, which is attenuated after processing by the MME scheme.

Similarly, most artifacts due to internal multiple reflections, indicated by the red arrows in Figure 6c, are successfully predicted. Correspondingly, they are removed in the image from the multiple-attenuated data set as shown in Figure 6b. Besides, the continuity of structures indicated by the green arrows numbered 1 and 2 has been improved and structures numbered 3 and 4 have been successfully recovered. This is due to the recovery of the canceled primary reflections after internal multiple reflection elimination by the MME scheme. Especially in the zones indicated by the green boxes in Figure 6a and 6b, most artifacts due to internal multiple reflections have been successfully removed and the continuity of the synclinal reflectors has been greatly improved.

DISCUSSION

As shown in the "Field example" section, the MME scheme successfully removes or attenuates most internal multiple reflections. Several primary reflections canceled by internal multiple reflections are recovered, and, correspondingly, the related structures are present in the image as shown in Figure 6. From the previous study in Verschuur and Berkhout (2005), where the IME scheme was applied to the same field data set, most internal multiple reflections removed by the MME scheme were effectively attenuated by the IME scheme. However, the canceled primary reflections indicated by the green arrows in Figure 2 could not be recovered with the IME scheme because of adaptive subtraction, which is based on the minimum-energy criterion. Therefore, we surmise that other schemes that apply adaptive subtraction, such as ISS-based schemes, can possibly attenuate internal multiple reflections that are removed by the MME scheme but cannot handle scenarios in which internal multiple reflections overlap with primary reflections.

The 2D field data set used here as an example is measured from an area with a deep ocean bottom. The deep water helps in reducing the mismatch in amplitude of the 2D MME scheme that is necessarily applied to a 3D line data set. The second advantage of deep water is the fact that the early arrivals of the measured data set is free from free-surface-multiple reflections. High-quality denoising, source wavelet deconvolution, and near-offset trace interpolation

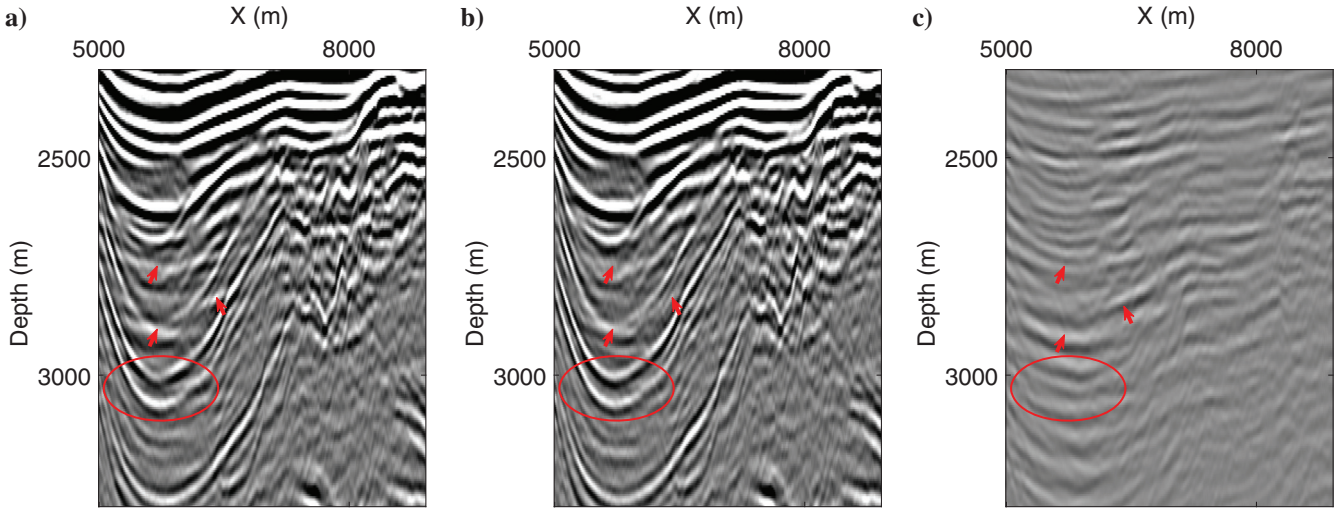

Figure 5. (a) The magnified portion of zone 2 in Figure 3a, (b) the magnified portion of zone 2 in Figure 3b, and (c) the difference between (a and b). The red circle and arrows highlight artifacts due to internal multiple reflections, which are removed after processing by the MME scheme.

are necessary for the successful application of the MME scheme. When the input data set has severe amplitude problems, the performance of the MME scheme is limited. The MME scheme was applied to a measured laboratory data set with variable quality. Because of amplitude errors in some parts of the data, some internal multiple reflections were effectively attenuated or removed by the MME scheme, whereas some were stronger and had opposite polarity after processing. These caused artifacts in the computed image. Combining the performance in the laboratory example and the field example here, we conclude that high-quality preprocessing is crucial for the success of the MME scheme.

The performance of this field data set validates the success of the MME scheme. Previous filter functions can be used as initial estimates for every new time instant. This feature makes the MME scheme an affordable method to remove internal multiple reflections before migration.

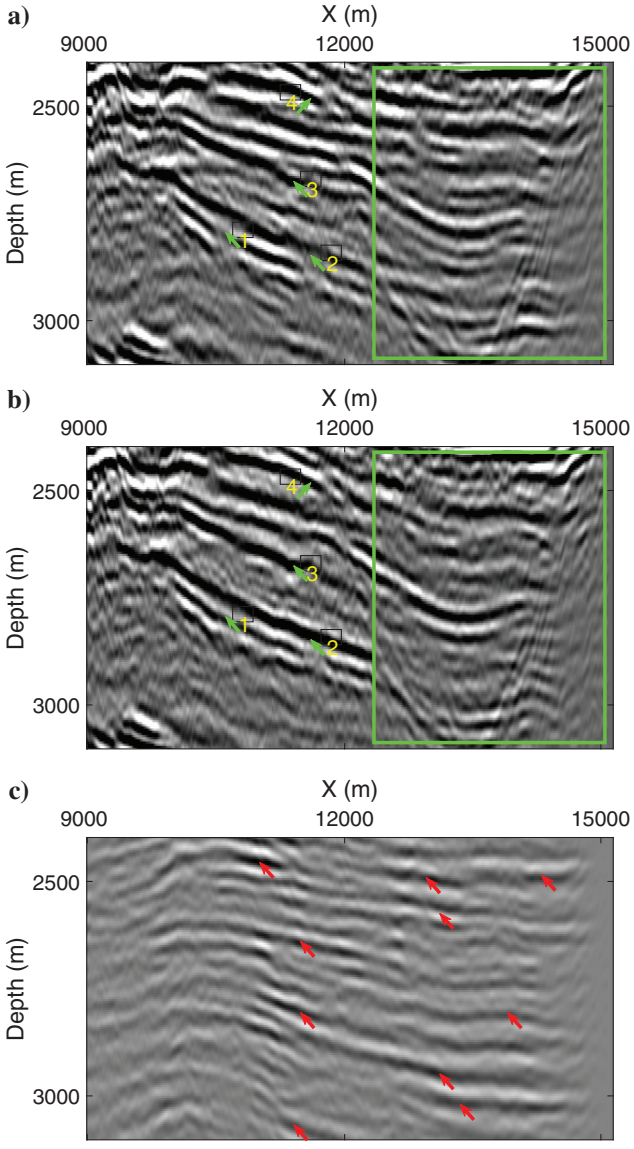

Figure 6. (a) The magnified portion of zone 3 in Figure 3a, (b) the magnified portion of zone 3 in Figure 3b, and (c) the difference between (a and b). The red arrows indicate artifacts due to internal multiple reflections. The green arrows indicate structures recovered, and the green boxes indicate the zone where most artifacts are removed by the MME scheme.

CONCLUSION

We have applied the MME scheme to a measured field data set to evaluate its performance. The field example shows that most internal multiple reflections are successfully eliminated and because of the independence from adaptive subtraction, the primary reflections that are canceled by internal multiple reflections are also recovered by the MME scheme. Given the successful application to the field data set, we think that the MME scheme is an appropriate method for removal of internal multiple reflections without model information or adaptive subtraction. We expect that the MME scheme can be widely used in geophysical exploration and monitoring of subsurface processes.

ACKNOWLEDGMENTS

This work is part of the Open Technology Program with project number 13939, which is financed by NWO Domain Applied and Engineering Sciences. We would like to thank J. Shragge, A. Kaslilar, M. Ravasi, and the two anonymous reviewers for their valuable suggestions.

DATA AND MATERIALS AVAILABILITY

Data associated with this research are available and can be obtained by contacting the corresponding author.

REFERENCES

Araújo, F. V., A. B. Weglein, P. M. Carvalho, and R. H. Stolt, 1994, Inverse scattering series for multiple attenuation: An example with surface and internal multiples: 64th Annual International Meeting, SEG, Expanded Abstracts, 1039–1041, doi: 10.1190/1.1822691.

Berkhout, A. J., 2014, Review paper: An outlook on the future of seismic imaging — Part 2: Full-wavefield migration: Geophysical Prospecting, **62**, 931–949, doi: 10.1111/1365-2478.12154.

Berkhout, A. J., and D. J. Verschuur, 1997, Estimation of multiple scattering by iterative inversion — Part 1: Theoretical considerations: Geophysics, **62**, 1586–1595, doi: 10.1190/1.1444261.

Brown, M. P., and A. Guitton, 2005, Least-square joint imaging of multiples and primaries: Geophysics, **70**, no. 5, S79–S89, doi: 10.1190/1.2052471.

Davydenko, M., and D. J. Verschuur, 2018, Including and using internal multiples in closed-loop imaging — Field data examples: Geophysics, **83**, no. 4, R297–R305, doi: 10.1190/geo2017-0533.1.

Kabir, M. M. N., and D. J. Verschuur, 1995, Restoration of missing offsets by parabolic radon transform: Geophysical Prospecting, **43**, 347–368, doi: 10.1111/j.1365-2478.1995.tb00257.x.

Löer, K., A. Curtis, and G. A. Meles, 2016, Relating source-receiver interferometry to an inverse-scattering series to derive a new method to estimate internal multiples: Geophysics, **81**, no. 3, Q27–Q40, doi: 10.1190/geo2015-0330.1.

Lu, S., D. N. Whitmore, A. A. Valenciano, and N. Chemingui, 2015, Separated-wavefield imaging using primary and multiple energy: The Leading Edge, **34**, 770–778, doi: 10.1190/tle34070770.1.

Luo, Y., P. G. Kelamis, S. Huo, G. Sindi, S. Hsu, and A. B. Weglein, 2011, Elimination of land internal multiples based on the inverse scattering series: The Leading Edge, **30**, 884–889, doi: 10.1190/1.3626496.

Matson, K., D. Corrigan, A. Weglein, C. Young, and P. Carvalho, 1999, Inverse scattering internal multiple attenuation: Results from complex synthetic and field data examples: 89th Annual International Meeting, SEG, Expanded Abstracts, 1060–1063, doi: 10.1190/1.1820681.

Meles, G., K. Löer, M. Ravais, A. Curtis, and C. A. da Costa Filho, 2015, Internal multiple prediction and removal using Marchenko autofocusing and seismic interferometry: Geophysics, **80**, no. 1, A7–A11, doi: 10.1190/geo2014-0408.1.

Slob, E., K. Wapenaar, F. Broggini, and R. Snieder, 2014, Seismic reflector imaging using internal multiples with Marchenko-type equations: Geophysics, **79**, no. 2, S63–S76, doi: 10.1190/geo2013-0095.1.

Staring, M., R. Pereira, H. Douma, J. van der Neut, and K. Wapenaar, 2018, Source-receiver Marchenko redatuming on field data using an adaptive double-focusing method: Geophysics, **83**, no. 6, S570–S590, doi: 10.1190/geo2017-0796.1.

Ten Kroode, P. E., 2002, Prediction of internal multiples: Wave Motion, **35**, 315–338, doi: 10.1016/S0165-2125(01)00109-3.

van der Neut, J., and K. Wapenaar, 2016, Adaptive overburden elimination with the multidimensional Marchenko equation: Geophysics, **81**, no. 5, T265–T284, doi: 10.1190/geo2016-0024.1.

van Groenestijn, G. J. A., and D. J. Verschuur, 2009, Estimating primaries by sparse inversion and application to near-offset data reconstruction: Geophysics, **74**, no. 3, A23–A28, doi: 10.1190/1.3111115.

Verschuur, D. J., and A. Berkhout, 2005, Removal of internal multiples with the common-focus-point (CFP) approach — Part 2: Application strategies and data examples: Geophysics, **70**, no. 3, V61–V72, doi: 10.1190/1.1925754.

Verschuur, D. J., and A. J. Berkhout, 2011, Seismic migration of blended shot records with surface-related multiple scattering: Geophysics, **76**, no. 1, A7–A13, doi: 10.1190/1.3521658.

Verschuur, D. J., A. Berkhout, and K. Wapenaar, 1992, Adaptive surface-related multiple elimination: Geophysics, **57**, 1166–1177, doi: 10.1190/1.1443330.

Wang, Y., Y. Zheng, Q. Xue, X. Chang, T. W. Fei, and Y. Luo, 2017, Reverse time migration of multiples: Reducing migration artifacts using the wavefield decomposition imaging condition: Geophysics, **82**, no. 4, S307–S314, doi: 10.1190/geo2016-0354.1.

Wang, Y., Y. Zheng, L. Zhang, X. Chang, and Z. Yao, 2014, Reverse time migration of multiples: Eliminating migration artifacts in angle domain common image gathers: Geophysics, **79**, no. 6, S263–S270, doi: 10.1190/geo2013-0441.1.

Wapenaar, K., J. Thorbecke, J. van der Neut, F. Broggini, E. Slob, and R. Snieder, 2014, Marchenko imaging: Geophysics, **79**, no. 3, WA39–WA57, doi: 10.1190/geo2013-0302.1.

Weglein, A. B., F. A. Gasparotto, P. M. Carvalho, and R. H. Stolt, 1997, An inverse scattering series method for attenuating multiples in seismic reflection data: Geophysics, **62**, 1975–1989, doi: 10.1190/1.1444298.

Whitmore, N. D., A. A. Valenciano, and W. Sollner, 2010, Imaging of primaries and multiples using a dual-sensor towed streamer: 80th Annual International Meeting, SEG, Expanded Abstracts, 3187–3192, doi: 10.1190/1.3513508.

Zhang, L., and E. Slob, 2019, Free-surface and internal multiple elimination in one step without adaptive subtraction: Geophysics, **84**, no. 1, A7–A11, doi: 10.1190/geo2018-0548.1.

Zhang, L., and M. Staring, 2018, Marchenko scheme based internal multiple reflection elimination in acoustic wavefield: Journal of Applied Geophysics, **159**, 429–433, doi: 10.1016/j.jappgeo.2018.09.024.

Zhang, L., J. Thorbecke, K. Wapenaar, and E. Slob, 2019a, Transmission compensated primary reflection retrieval in data domain and consequences for imaging: Geophysics, **84**, no. 4, Q27–Q36, doi: 10.1190/geo2018-0340.1.

Zhang, L., J. Thorbecke, K. Wapenaar, and E. Slob, 2019b, Data-driven internal multiple elimination and its consequences for imaging: A comparison of strategies: Geophysics, **84**, no. 5, S365–S372, doi: 10.1190/geo2018-0817.1.